The new RD52 (DREAM) fiber calorimeter

Richard Wigmans[1]

Department of Physics
Texas Tech University
Lubbock, TX 79409-1051, U.S.A.

E-mail: wigmans@ttu.edu

Abstract. Simultaneous detection of the Čerenkov light and scintillation light produced in hadron showers makes it possible to measure the electromagnetic shower fraction event by event and thus eliminate the detrimental effects of fluctuations in this fraction on the performance of calorimeters. In the RD52 (DREAM) project, the possibilities of this dual-readout calorimetry are investigated and optimized. In this talk, the first test results of prototype modules for the new full-scale fiber calorimeter are presented.

1. Introduction - Dual-Readout Calorimetry

High-precision measurements of the four-vectors of fragmenting quarks and gluons will be increasingly important in experiments at the high-energy frontier, and in particular at a future Linear electron-positron Collider. RD52 is a *generic* detector R&D project, carried out at CERN by the DREAM Collaboration, in which we investigate, and to the extent possible eliminate, the factors that prevent calorimetric measurements of the four-vectors of jets and single hadrons with the same level of precision as for electrons and photons.

The key aspect of DREAM detectors is the simultaneous measurement of scintillation light and Čerenkov light generated in the shower development process. By comparing these two signals, the electromagnetic shower fraction can be measured event by event, and the effects of fluctuations in this fraction on the hadronic calorimeter performance can be eliminated.

The merits of this technique were first illustrated with a calorimeter in which the two signals were provided by two different types of optical fibers. More recently, we have also concentrated on crystals ($PbWO_4$, BGO and BSO), which have the potential of eliminating (or at least reducing) the contributions of the next two important sources of fluctuations: photoelectron statistics and sampling fluctuations. We have identified and investigated four different methods to split the signals from such crystals into scintillation and Čerenkov components. These results have been reported at previous editions of the CALOR conference series [1, 2] and in the scientific literature [3].

At this conference, Gabriella Gaudio has reported our recent results on electromagnetic dual-readout calorimetry with two different matrices of crystals that are large enough to contain em showers at a sufficient level [4]. In this talk, I will describe the progress on the new dual-readout fiber calorimeter that is being built and tested by the RD52 Collaboration. In Section 2, I describe the rationale for the design choices that were made, and in Section 3, I present the first results of beam tests of prototype modules of this calorimeter.

[1] Talk presented on behalf of the RD52 Collaboration (Gagliari, Cosenza, Pavia, Pisa, Roma, Iowa State, TTU)

2. Why a Copper-Fiber Calorimeter?

The energy resolution of a calorimeter is determined by *fluctuations*. This means, for example, that the fact that two thirds of the energy of a jet is typically carried by charged particles is completely irrelevant in that context. Even though this jet component can be measured with very high precision, a detector that *only* would be sensitive to this component would not be capable of measuring jet energies with a precision better than 20%, at *any energy*, because of event-to-event fluctuations in this fraction [5]. Fluctuations that determine the hadronic energy resolution of a calorimeter system include:

(i) Fluctuations in the energy fraction carried by the *electromagnetic shower component*, $f_{\rm em}$. These fluctuations are non-Gaussian and typically dominate the hadronic energy resolution of the calorimeters used in the current generation of experiments, especially at high energies. They can be eliminated either by making the calorimeter intrinsically compensating ($e/h = 1$), or by measuring the value of $f_{\rm em}$ event by event. DREAM calorimeters use the latter approach, which offers essentially the same advantages as compensation, without the inherent limitations in terms of the choice of absorber medium, sampling fraction, integration time and volume [6].

(ii) Fluctuations in the *invisible* energy. These are dominated by the nuclear binding energy losses in the numerous nuclear reactions through which the shower absorption proceeds. Efficient detection of the nuclear reaction products, and in particular of the abundantly produced neutrons, makes it possible to limit the effects of these fluctuations on the hadronic energy resolution. These fluctuations determine the ultimate resolution limit one may hope to achieve ($\sim 15\%/\sqrt{E}$ [6]), and also explain the different single-hadron resolutions obtained with the ZEUS [7] and D0 [8] calorimeters. These devices were both (approximately) compensating and stochastic fluctuations contributed similarly to the resolution. Yet, the plastic scintillator active medium of ZEUS was a much more efficient detector of the nuclear reaction products than the liquid argon used in D0, which led to a much better resolution for ZEUS.

(iii) *Stochastic* fluctuations. In the DREAM calorimeters, these include sampling fluctuations and Poisson fluctuations in the number of Čerenkov photoelectrons.

Based on our results, we believe that a copper-fiber dual-readout calorimeter offers the best opportunities to achieve hadronic energy resolutions at the 1% level. The first two types of fluctuations are minimized by design in such a calorimeter, and the stochastic fluctuations can be reduced considerably compared to the original DREAM calorimeter, in which sampling fluctuations and Poisson fluctuations in the numbers of Čerenkov photoelectrons each contributed $\sim 35\%/\sqrt{E}$ to the measured

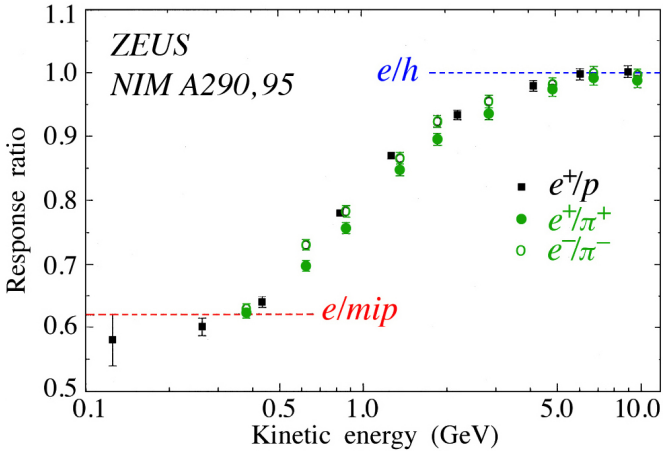

Figure 1. The response of the (compensating) ZEUS uranium/plastic-scintillator calorimeter to low-energy hadrons [10].

resolution, and we expect to bring this down to $\sim 10\%/\sqrt{E}$. One could argue that these stochastic fluctuations could be reduced even more in homogeneous dual-readout calorimeters. However, in such calorimeters fluctuations in invisible energy would be much larger because of the insensitivity of such devices to the nuclear shower component, and thus dominate the resolution. Using complementary arguments, Don Groom has shown that the performance of such devices, even if the funds could be found to build them, would most likely be disappointing [9].

Also the choice of copper as absorber material is an essential ingredient of our plans. As mentioned above, one advantage of the dual-readout technique over intrinsically compensating calorimeters is the fact that it allows the use of low-Z absorber material such as copper. This is especially important for obtaining excellent energy resolutions for *jets*. This is illustrated in Figure 1, which shows the response of the ZEUS calorimeter to low-energy single hadrons, relative to the response to electrons. For energies above 5 GeV, this response ratio is 1.0, since the calorimeter is compensating. The strong non-linearity observed for lower-energy hadrons is a consequence of the fact that, as the energy decreases, an increasing fraction of the hadrons do not develop showers, but rather range out, *i.e.,* behave as muons. In comparison with mips, em showers are inefficiently sampled in calorimeters with high-Z absorber material [6]. In the ZEUS calorimeter, which used depleted uranium (^{238}U) as absorber material, the e/mip ratio was only ~ 0.6. And since soft hadrons are typically a major component of fragmenting quarks and gluons, the jet resolution in ZEUS was significantly worse than for single hadrons. This effect could be avoided in dual-readout calorimeters that use copper as absorber material, since the e/mip value is in that case ~ 0.9.

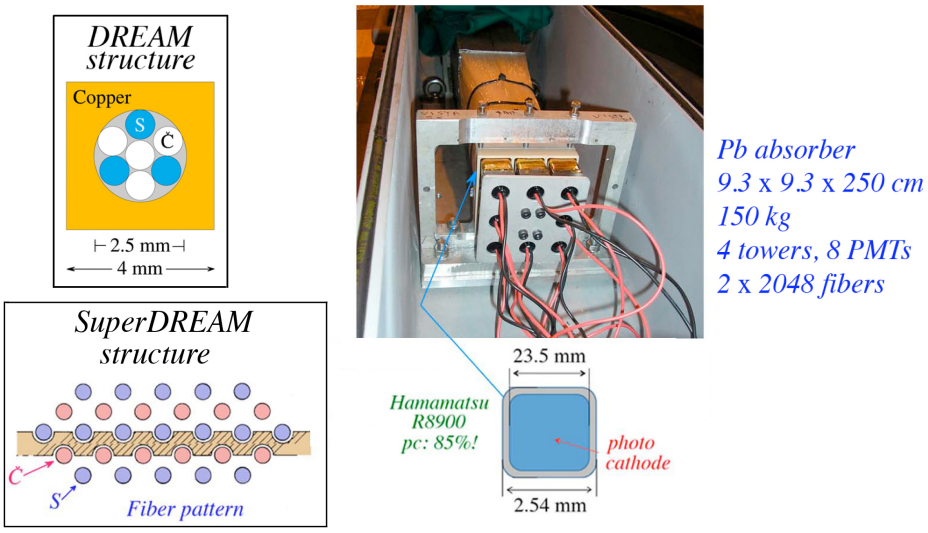

Figure 2. The fiber patterns used in the original DREAM calorimeter and in the new SuperDREAM modules (*left diagrams*). Also shown is how the fibers sticking out from the rear end of the module are connected to 8 PMTs. These PMTs (Hamamatsu R8900) have a very large effective photocathode area, 85% of the outer envelope of the tube.

Our design to limit the contributions of stochastic fluctuations as much as possible is based on the following elements:

- Embed the fibers *individually* in the absorber structure. In the original DREAM modules, seven fibers were grouped together and split at the rear end of the module into C and S bunches. This difference is illustrated in Figure 2.
- Maximize the *fiber density* in the detector modules. The limit in this respect is determined by the fact that the readout structure has to fit within the detector envelop. To that end, we selected PMTs with a large ratio of the effective photocathode area and the outside perimeter. In the R8900

Hamamatsu tubes this ratio is 85%, which allowed us to increase the fiber packing fraction by more than a factor of two compared to the original DREAM module (Figure 2).

- Use Čerenkov fibers with a considerably *larger numerical aperture* (N.A.) than the quartz ones used in the DREAM module. Initially, we had selected multi-clad polystyrene (PS) Kuraray fibers for this purpose, which have a N.A. of 0.72. However, beam tests of the first SuperDREAM module equipped with these fibers revealed an unacceptably strong light attenuation ($\lambda_{\rm att} \approx 3$m), as a result of Rayleigh scattering in the PS. We then decided to use PMMA based fibers instead. These fibers, made by Mitsubishi, have a N.A. of 0.50, but thanks to the much longer light attenuation length the signals were found to be about twice as large as in the PS case (Figure 3). A direct measurement

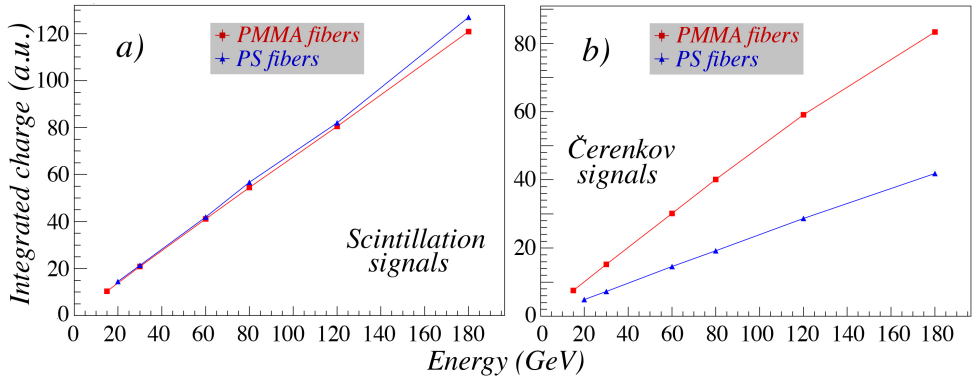

Figure 3. The average electron signal as a function of energy for a SuperDREAM module equipped with polystyrene and another module equipped with PMMA fibers for the detection of the Čerenkov light. The scintillating fibers were of the same type in both modules. The 8 readout PMTs were exactly the same in both modules. Shown are the results for the scintillation (a) and the Čerenkov (b) signals.

of the Čerenkov light yield gave 32 photoelectrons per GeV deposited energy in the PS module. In the PMMA module, this light yield was a factor two larger. For comparison, we mention that the Čerenkov light yield in the original DREAM module was only 8 photoelectrons per GeV. We expect to be able to increase this number to well over 100 p.e./GeV in the final SuperDREAM modules.

- The Čerenkov light yield is further increased by aluminizing the upstream ends of the fibers and by using PMTs with a super-bialkali photocathode.

We expect to test a calorimeter module in which all these improvements have been implemented in July.

3. Results of beam tests of prototype modules

The first two prototype modules, results of which are shown in Figure 3, were build with lead as absorber material. The absorber structure needed for the high-sampling-frequency SuperDREAM calorimeter is relatively easy to extrude using this material. In the meantime, we have also found a way to make this absorber structure out of copper, and the first two copper modules are being prepared for our beam tests in July. The results shown in this section were obtained with the lead module equipped with PMMA Čerenkov fibers. Figure 4 shows the em energy resolution in the Čerenkov channel as a function of energy. For comparison, the published resolution obtained with the original DREAM module [11] is shown as well. The improvement is especially important at the highest energies, due the absence of a significant deviation from $E^{-1/2}$ scaling (the so called "constant term"). Further improvements may be expected as a result of the use of copper absorber, fiber aluminization and better shower containment.

Measurements of the em energy resolution are a good way to assess the reduction obtained in the stochastic fluctuations, since such fluctuations are the only ones that matter in a well designed sampling calorimeter. However, since SuperDREAM is also intended to be a very good hadron calorimeter, we also

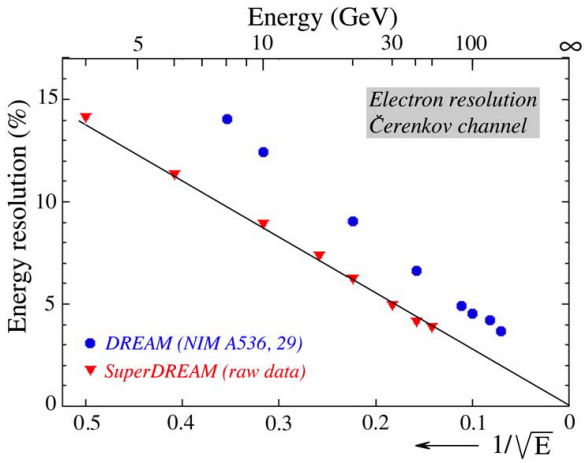

Figure 4. Comparison of the em energy resolution in the Čerenkov channel, measured with the first SuperDREAM modules and with the original DREAM calorimeter [11].

made some measurements with hadrons. Of course, side leakage is a major factor for the performance in that case. In order to limit the effects of such leakage out of the 150 kg calorimeter module, we surrounded it by 16 plastic scintillator counters (see Figure 5), which provided a crude measurement of the energy of the particles escaping from the calorimeter. Results of these measurements are shown

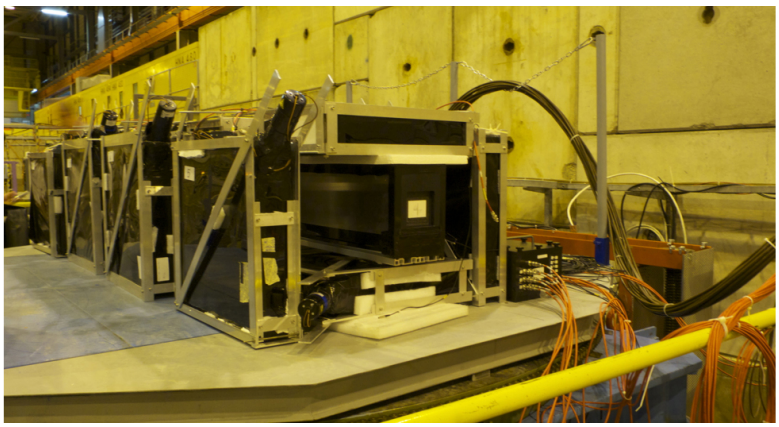

Figure 5. The setup in which individual SuperDREAM modules are being tested in the H8 beam. The module is contained in a box surrounded by 16 leakage counters.

in Figure 6. Figures 6a and 6b show the scintillation signal distribution for 180 GeV pions sent into this module and the (anti-)correlation between these signals and those observed in the leakage shield, respectively. The virtue of the dual-readout principle is illustrated in Figure 6c, which shows a scatter plot of the (corrected) scintillation signal versus the Čerenkov/scintillation signal ratio. As expected, the smaller this ratio, the smaller $f_{\rm em}$ and, therefore, the smaller the scintillation signal. After an event-by-event correction based on the measured $f_{\rm em}$ value, this scatter plot is converted into the one shown in Figure 6d, and the projection of this scatter plot on the horizontal axis (Figure 6e) yields a Gaussian distribution with approximately the right energy and a fractional width of less than 5%. This is an encouraging result, which we expect to improve considerably at the end of this year, when all available SuperDREAM modules will be assembled to form a calorimeter with a mass of $\sim$ 2000 kg, and tested in hadron beams at CERN. Figure 7 shows some pictures of the production of SuperDREAM modules at the University of Pavia.

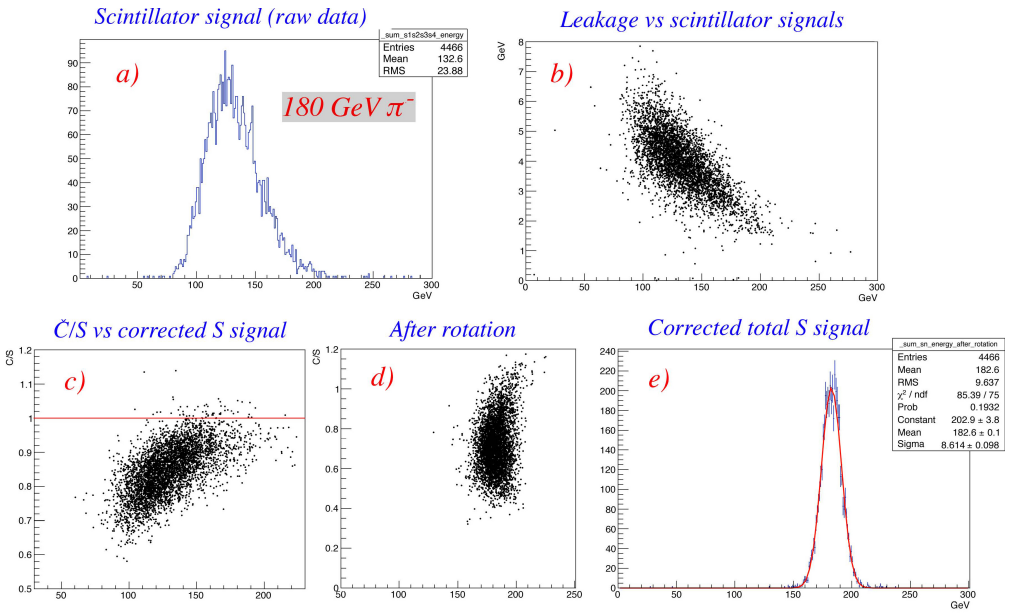

Figure 6. First measurements of pions in a single module of the new SuperDREAM fiber calorimeter, surrounded by leakage detectors. See text for details.

A crucial aspect of this type of calorimeter is its *longitudinally unsegmented* structure. This allows a compact construction and avoids the complications usually encountered with the intercalibration of different longitudinal sections in a longitudinally segmented detector system. Potential disadvantages of this structure concern the identification of electrons and photons, and the measurement of the direction of neutral incoming particles.

However, a fine lateral segmentation combined with information on the detailed time structure of

Figure 7. New SuperDREAM modules under construction at the University of Pavia (top), and at INFN Pisa (bottom). The Pavia modules use lead as absorber material, the Pisa ones copper.

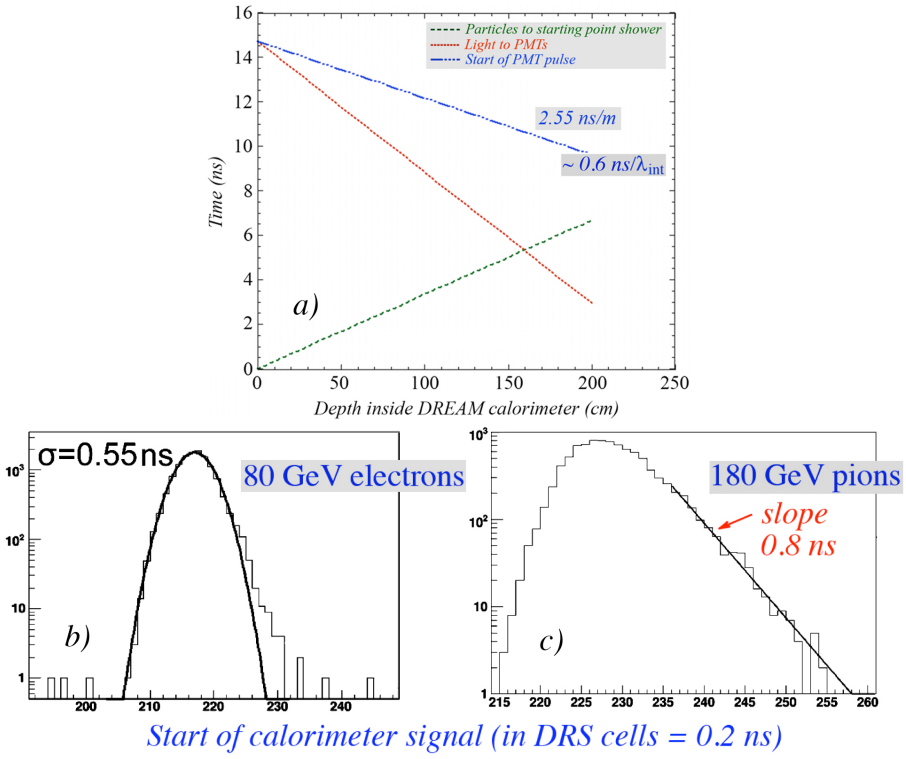

Figure 8. Principle of the measurement of the depth of the light production through the starting time of the signal (a). Distribution of the starting times of signals from 80 GeV electrons (b) and 180 GeV pions (c) in the fiber calorimeter.

the events greatly alleviates these problems. Measurement of the time structure of the signals makes it possible to obtain crucial information about the depth at which the light is produced. By using the fact that light travels at a speed of c/n in the fibers, while the particles producing the light travel at c, the starting time of the signals makes it possible to measure the depth at which the light is produced, as illustrated in Figure 8a. The deeper the light is produced, the earlier the PMT signal starts. The distribution of the starting points of the signals generated by 80 GeV electron showers (Figure 8b) indicates a time resolution of 0.55 ns, which corresponds to a depth resolution of $\sim$ 20 cm (Figure 8a). The varying depth at which pion showers start is clearly illustrated in Figure 8c.

This feature makes it possible to correct for small effects of light attenuation in the fibers. It is also an important tool for electron/photon identification in this type of calorimeter. As demonstrated by SPACAL, a simple measurement of the duration of the signals (the full width at 20% of the amplitude) made it possible to separate electrons from pions at the 99.99% level [12]. Finally, the time structure is an important tool for measuring the neutron contribution to the scintillation signals [13].

We measure the time structure of each calorimeter signal with a Domino Ring Sampler chip [14]. An array of 1024 switching capacitors samples the input signal at a frequency determined by the Domino Wave. Once a trigger is received, the capacitors are sequentially read out by a pipeline 12-bit ADC, starting from the leading edge of the trigger signal, moving backward. In this way, the time history of the signal is stored in the DRS output, while the trigger itself is stored in a DRS channel. In our measurements, we operate this circuit at 5 GHz, for a time resolution of 0.2 ns. Figure 8 clearly illustrates the benefits of this approach.

References

[1] Wigmans R 2009, Proceedings of the XIIIth Conference on Calorimetry in High Energy Physics, J. Phys. Conf. Series **160**, 012018; *ibid.* Gaudio G, 012068; Carosi R, 012069; Voena C, 012070: Pinci D, 012071; Hauptman J, 012072.

[2] Gaudio G 2011, Proceedings of the XIVth Conference on Calorimetry in High Energy Physics, J. Phys. Conf. Series **293**, 012006; *ibid.* Hauptman J, 012080.

[3] Akchurin N *et al.* 2005 Nucl. Instr. and Meth. **A537**, 537; *ibid.* **A550**, 185; **A581**, 643; **A595**, 359; **A621**, 212; **A638**, 47.

[4] Gaudio G 2012, Contribution to these Proceedings.

[5] Lobban O, Shriharan A and Wigmans R 2002, Nucl. Instr. and Meth. **A495**, 107.

[6] Wigmans R 2000, *Calorimetry - Energy Measurement in Particle Physics*, International Series of Monographs on Physics, vol. 107, Oxford University Press.

[7] Behrens U *et al.* 1990, Nucl. Instr. and Meth. **A289**, 115.

[8] Aronson S *et al.* 1988, Nucl. Instr. and Meth. **A269**, 492.

[9] Groom D 2012, Contribution to these Proceedings.

[10] Andresen A *et al.* 1990, Nucl. Instr. and Meth. **A290**, 95.

[11] Akchurin N *et al.* 2005, Nucl. Instr. and Meth. **A536**, 29.

[12] Acosta D *et al.* 1991, Nucl. Instr. and Meth. **A302**, 36.

[13] Akchurin N *et al.* 2009, Nucl. Instr. and Meth. **A598**, 422.

[14] Ritt S *et al.*2010 Nucl. Instr. and Meth. **A623**, 486.